VERY HIGH PRECISION VLBI ASTROMETRY OF THE S5 POLAR CAP SAMPLE SOURCES

IVÁN MARTÍ-VIDAL, JON MARCAIDE, JOSE C. GUIRADO
Departament d'Astronomia i Astrofísica, Universitat de Valencia, E-46100 Burjassot, Valencia, SPAIN

Abstract: We report on the first astrometric analysis of the thirteen extragalactic radio sources of the complete S5 polar cap sample at 15.4 GHz. We describe new algorithms developed to facilitate the use of differential phase delay in global astrometric observations. From this global fit, we obtain preliminary estimates of source positions with precisions that range from 50 to 100 μas at 15.4 GHz.

1 Introduction

In the last years, we have carried out a series of VLBI observations, using the Very Long Baseline Array (VLBA) aimed at studying the absolute kinematics of a complete sample of extragalactic radio sources using astrometric techniques at 8.4, 15.4, and 43 GHz. The target of our programme is the "complete S5 polar cap sample", consisting on thirteen radio sources from the S5 survey [1, 2]. All sources in this sample have large flux densities and well defined ICRF (*International Celestial Reference Frame*) positions. The relative source separations, less than about 15 deg, allow for astrometric precisions in the range of 20 to 100 μas, depending of the observing frequency. We described the goals of our astrometric programme in [3] and presented VLBA maps obtained at two different epochs at 8.4 GHz [3] and 15.4 GHz [4]. Here, we report on the first phase-delay astrometric results of this programme. We describe in detail the algorithm from which we derived, automatically, the $2\pi-$ambiguities inherent to the phase-delay observable and discuss the contribution of differential observables for sources distributed over a large portion of the sky. Our results are essential for future improvements of the ICRF definition and future combination of radio positions with optical positions from space-based astrometric missions.

2 Observations and maps

We observed the complete S5 polar cap sample (see Figure 1) at 15.4 GHz on 19 August 2004 using the complete Very Long Baseline Array (VLBA) for 24 hr. We observed blocks of 3 or 4 radio sources, with duty cycles of about 6 min, for about 2 hr. On-source scans were 60 sec long, with a small time gap (10-20 sec) to slew the VLBA antennae. This observing mode resulted in a total observation time for each radio source of about 4 hr (see Figure 1). Data were cross-correlated at the National Radio Astronomy Observatory (NRAO) facility in Socorro. Manual phase calibration, visibility amplitude calibration (using system temperatures and gain curves from each antenna) and fringe fitting at the correlation position were made with the NRAO Astronomical Image Processing System (AIPS). For mapping, we transferred the data into the Caltech imaging program Difmap [5] and made several iterations of phase and gain self-calibration. We show the maps obtained in Figure 2.

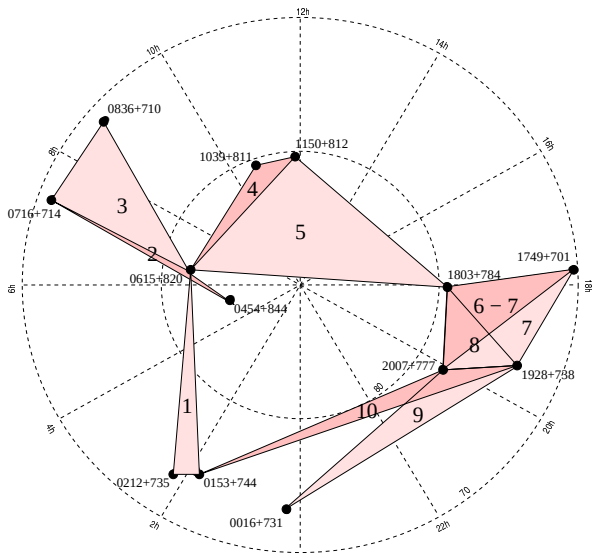

Figure 1: Sky distribution of polar cap sample sources. The sources in the vertices of each shadowed area are repeatedly observed with a duty cycle of about 6 min. These sequential observations constitute a block of observations. The numbers associated to the shadowed areas represent the chronological order of the blocks of observations.

3 Astrometric Analysis

We performed a differential astrometry analysis similar to earlier analyses (e. g. [6, 7, 8]), but with some substantial differences. We outline the main steps followed in the analysis: (i) we used AIPS to obtain the group delay, phase delay, and rate from each observation of each of the thirteen sources; (ii) we subtracted all the contributions from the structure of the sources referring all the astrometric observables to the phase center of the maps of the sources shown in Figure 2; (iii) we predicted, via a precise astrometric model, the number of cycles of phase between successive observations of the same source to permit us to "connect" the phase delays (e. g. [6, 7, 8]); (iv) we refined this phase-delay connection using an algorithm that imposes the nullity of all the closure phases (see section 3.1 for details); (v) we formed differenced phase delays between all the sources observed in the same block of observations (see Figure 1); and (vi) we estimated the relative positions of the thirteen sources via a global weighted-least-squares analysis to the undifferenced and differenced data. We used the *University of Valencia Precision Astrometry Package* (UVPAP), an extensively improved version of the VLBI3 program [9]. The details of UVPAP will be described in detail in [10].

Source	$\mathbf{S}_{tot}$ mJy	$\mathbf{S}_{peak}$ mJy/beam	**rms level** mJy/beam
0016+731	1170	1160	0.56
0153+744	269	138	0.34
0212+735	2478	1720	0.95
0454+844	264	183	0.44
0615+820	396	156	0.20
0716+714	1345	1205	0.59
0836+710	1456	786	0.80
1039+811	1119	863	0.43
1150+812	1621	1029	0.33
1749+701	705	557	0.43
1803+784	1494	1002	0.28
1928+738	3018	1712	0.47
2007+777	988	571	0.23

Table 1: Total flux density, peak flux density, and rms of the maps for all the sources of the sample.

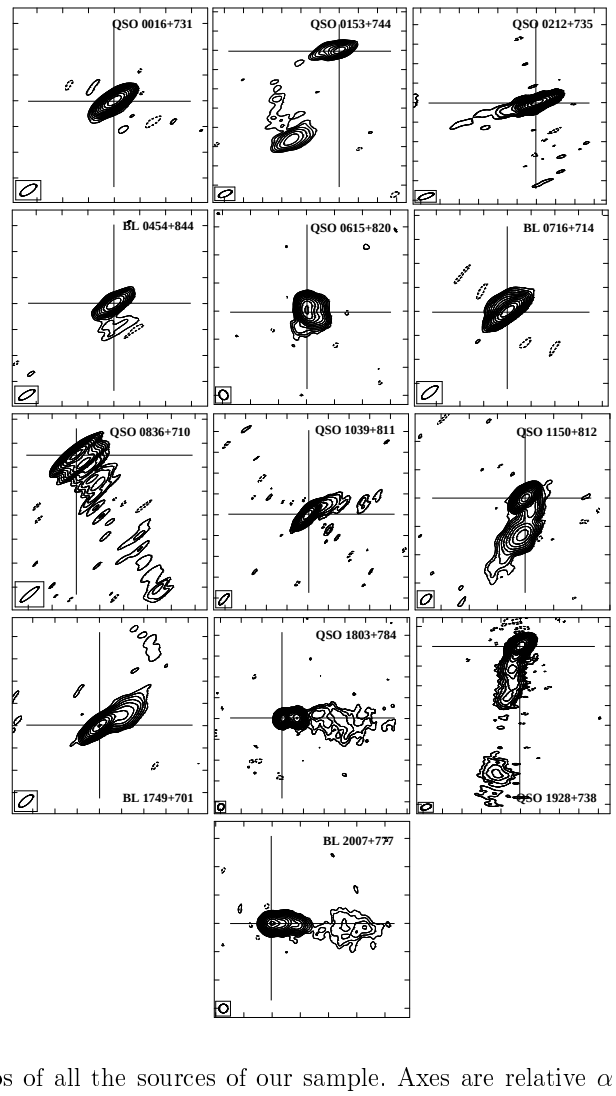

Figure 2: Maps of all the sources of our sample. Axes are relative α and δ (1 tick = 2 mas). Crosses indicate the phase center of the maps. Contours are (-3, 3, $3\sqrt{3}$, 9, $9\sqrt{3}$, ...) times the rms of each map (see table 1). FWHM of restoring beam is at bottom left of each map.

In step (iii) we used an accurate astrometric model of the geometry of our interferometric array and the propagation medium. The geometric parameters of our model relied on source coordinates, site coordinates, and daily values of the Earth orientation parameters (UT1-UTC, Earth's pole coordinates, and corrections to the model of the Earth's nutation in longitude and obliquity) provided by the International Earth Rotation Service (2004 IERS Annual Report) and interpolated at the time of our observations. Regarding the propagation medium, we modelled the tropospheric zenith delay at each station as a piecewise-linear function. A priori values at the nodes were calculated from local surface temperature, pressure, and humidity based on the Saastamoinen model [11]. We used the dry and wet Chao mapping functions [12] to determine the tropospheric delays at elevations other than the zenith. For the ionosphere, we used global ionospheric maps at the epoch of our observations derived from GPS data and generated by the Center for Orbit Determination in Europe (CODE). These maps (in IONEX format) provide the Earth's total electron content (TEC), that we transformed into delays over each station using the AIPS task TECOR.

3.1 Phase-Connection Algorithm

The astrometric model described in the previous section was used to predict the number of phase cycles (ambiguities) between consecutive observations of the same source by means of the residual delay rate: given that the average time separation between observations is $\sim$180 sec and the phase cycle at 15.2 GHz is $\sim$65 ps, the residual rates should be smaller than 0.36 ps/sec (65 ps/180 sec) to insure a good phase connection. In Figure 3 we plot the distribution of the residual rates of our observations. Rate residuals with absolute values larger than 0.36 ps/sec in the distribution of the phase cycles, most of them corresponding to longest baselines and weakest sources, are not uncommon. Thus, this preliminary phase connection is far from perfect and both time- and baseline-dependent phase cycles remain uncorrected in our data. In previous works, with less antennae and less sources (e. g. [7, 8]) these additional cycles could be corrected by inspection of the phase residuals. However, this procedure is unmanageable with the amount of data in our observations. Therefore, we have worked out an algorithm to automate the correction of these unmodelled phase cycles. The algorithm works as follows:

- For each source and observing time, we compute the closure phases corresponding to all triplets of antennae. From this particular set, we select the baseline most frequently occurring in the *non-zero* closure phases.
- We perform an *ambiguity check* on such baseline. By *ambiguity check*, we mean a shift of the phase-delays of that baseline by adding or subtracting

a phase-delay cycle. The first *check* performed is *positive* (i.e. addition of a cycle). We then compute the *score* corresponding to that *ambiguity check*. By *score*, we mean the number of closure phases approaching zero minus the number of closure phases distancing from zero after the *ambiguity check*.

- Afterwards, we perform a negative *ambiguity check* to the original data of the selected baseline (i.e. subtraction of a cycle). A new *score* is assigned to this new check.
- The *ambiguity check* finally selected is the one with highest *score*. We repeat this process until all the closure phases (i. e., closure phase-delays) are made zero for a source and time selected.

We apply this algorithm to all scans in our observations. Actually, to ease the work, for consecutive scans of the same source we apply the corrections found in the previous scan before performing the *ambiguity check*.

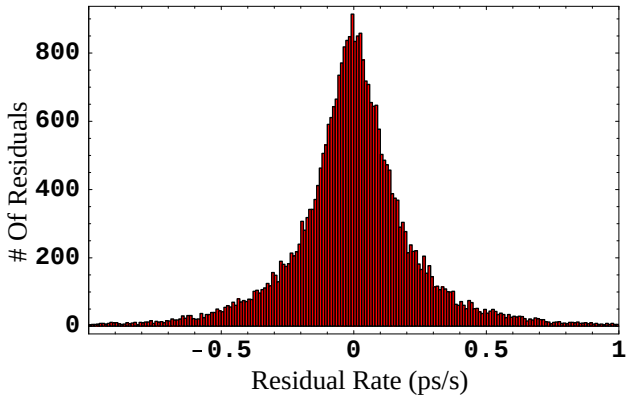

Figure 3: Distribution of the delay rate residuals for all the baselines and sources of our observations.

However, unmodelled cycles could still be left in our data if the corrections are antenna-based. Such cycles do not affect the phase closures and, thus, are completely transparent to the automatic connection algorithm described above. To correct these antenna-based ambiguities, we developed another algorithm based on a *smoothness criterion*, that analyzes variations between neighboring scans that are higher than a phase cycle. For each scan, the algorithm (i) finds such variations, (ii) analyzes if these jumps have an antenna-based structure,

and (iii) corrects the antenna-based phase cycle in the observations. We notice that the closure phases are not affected by this correction. We have tested this "automatic connector" with synthetic data, and found excellent results.

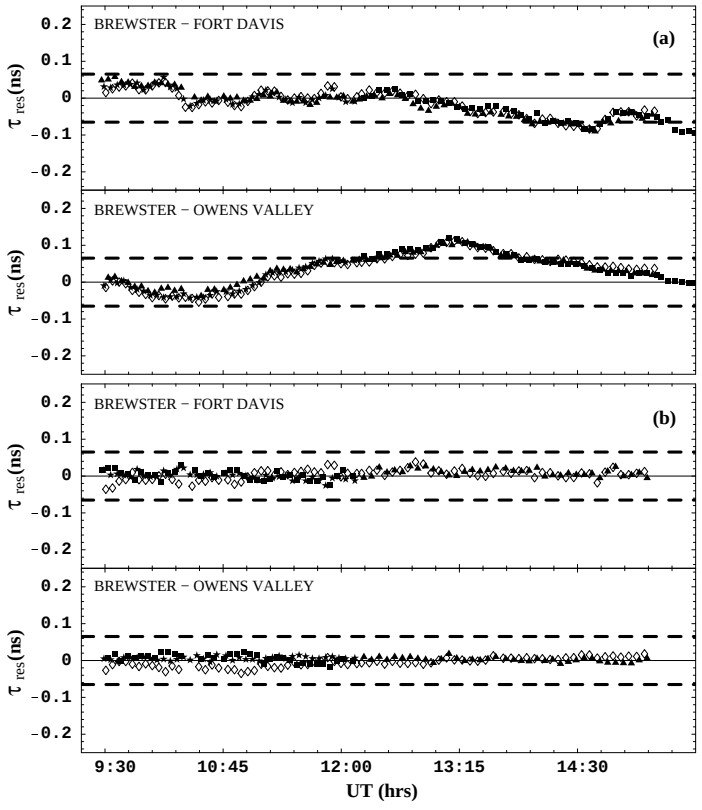

Figure 4: (a) Residuals of the connected phase delays for two selected baselines and some of the observed sources: 1803+784 (squares), 0615+820 (triangles), 1039+811 (stars) and 1150+812 (diamonds). (b) Differential residuals for the same baselines and sources as in (a): 0615+820 minus 1039+811 (squares), 0615+820 minus 1803+784 (triangles), 1039+811 minus 1150+812 (stars) and 0615+820 minus 1150+812 (diamonds). Dashed lines represent the delay of a 2π cycle ($\sim$ 65 ps). The data were weighted so that the reduced χ^2 per baseline and source is unity.

3.2 Differential Observables and Global Fit

Once the phase connection was completed, we computed the differential delays between the sources observed in the same blocks (see Figure 1). These differential delays are largely free from unmodelled effects of the troposphere, ionosphere, and antenna electronics (e. g. [13]).

We used both the differenced and undifferenced observations in the same (global) fit; the latter are included for the fit to remain sensitive to the antenna-dependent parameters (i. e., clock drifts and zenith delays). We fitted the positions of all the sources with respect to the phase center of 1803+784 (kept fixed in the fit) along with the tropospheric zenith delays, clock drifts, and constant clock offsets, for each antenna and source. For the computation of the parameter uncertainties, we let all the geometric parameters provided by IERS vary in the final fit, but assigning to them an a priori covariance according to their standard deviations (see [10] for details).

4 Results and Discussion

We have estimated the relative positions of all sources in the sample with respect to 1803+784.

We show in Figure 4 both the undifferenced and differenced residual phase delays corresponding to a selected set of baselines and sources. We notice in the differenced data the cancellation of systematic effects (probably unmodelled atmospheric effects) which can still be seen in the undifferenced data. We show preliminary results of the astrometric analysis, using the antennae of Brewster, North Liberty and Owens Valley, in table 2. We are currently developing further refinements of the geometric model and of the propagation medium to improve the residuals for the rest of antennae at certain times of the experiment. The final astrometric estimates of all the sources will be given and discussed elsewhere [10].

With these observations, we also intend to study the role of both the undifferenced and differenced observables in "global" astrometry. In fact, the relative weight between both sets of observables will determine the final uncertainties of our determinations. The use of the undifferenced data is necessary to track the clock drifts and atmospheric loading, but to the cost of a significant increment of the statistical error estimates. Finding a balance between the use of both types of observables will result in better and more robust astrometric determinations.

Source	$\Delta\alpha$ μas	$\Delta\delta$ μas
0016+731[1]	-3900 ± 400	-1820 ± 500
0153+744[1]	-1400 ± 200	3700 ± 200
0212+735[1]	-1200 ± 200	4000 ± 200
0454+844	-1380 ± 100	-690 ± 80
0615+820	-1950 ± 40	-130 ± 50
0716+714	-3270 ± 160	30 ± 120
0836+710	-4420 ± 150	-2770 ± 170
1039+811	-1080 ± 60	790 ± 60
1150+812	-760 ± 50	360 ± 50
1749+701	-3520 ± 50	3270 ± 120
1803+784	Reference	Reference
1928+738[1]	-9600 ± 70	-5600 ± 90
2007+777	840 ± 60	-1620 ± 60

Table 2: Preliminary results of our astrometric analysis relative to the ICRF positions (which coincide with the phase centers of the maps in Figure 2). The antennae used in the fit are Brewster, North Liberty and Owens Valley.
[1] We found high variations of the tropospheric delay during the observation of these sources. The correct modelling of such delay will further improve the results.

5 Conclusions

We report here the first astrometric results of our monitoring of the S5 polar cap at 15.4 GHz. Data from other epochs at other wavelenghts are also currently being analyzed. This multi-epoch, multi-frequency study will eventually provide results on the spectra and the absolute kinematics of all sources in the sample. Ultimately, we expect to provide a definitive test of the standard jet interaction model [14]. Additionally, our results will be an excellent complement for future μas-precise astrometry at optical wavelengths.

Acknowledgements: This work has been partially funded by Grants AYA2004-22045-E and AYA2005-08561-C03-03 of the Spanish DGICYT. The NRAO is a facility of the National Science Foundation operated under cooperative agreement by Associated Universities, Inc.

References

[1] Kühr H., Witzel A., Pauliny-Toth I.I.K., Nauber U. 1981, A&A 45, 367
[2] Eckart A., Witzel A., Biermann P., Johnston K.J., Simon R., Schalinski C., Kühr H. 1986, A&A 168, 17
[3] Ros E., Marcaide J.M., Guirado J.C., Pérez-Torres M.A. 2001, A&A 376, 1090
[4] Pérez-Torres M.A., Marcaide J.M., Guirado J.C., Ros E. 2004, A&A 428, 847
[5] Shepherd M.C., Pearson T.J., Taylor G.B. 1995, BAAS 26, 987
[6] Shapiro I.I., Wittels J.J., Counselman C.C., Robertson D.S., Whitney A.R., Hinteregger H.F., Knight C.A., Clark T.A., Hutton L.K., Niell A.E. 1979, AJ 84, 1459
[7] Guirado J.C., Marcaide J.M., Elosegui P., Ratner M.I.; Shapiro I.I., Eckart A., Quirrenbach A., Schalinski C.J., Witzel A. 1995, A&A 293, 613
[8] Ros E., Marcaide J.M., Guirado J.C., Ratner M.I., Shapiro I.I., Krichbaum T.P., Witzel A., Preston R.A. 1999, A&A 348, 381
[9] Robertson D.S. 1975, in *Geodetic and astrometric measurements with Very Long Baseline Interferometry*, Ph. D. Thesis, MIT
[10] Martí-Vidal I., Marcaide J.M., Guirado J.C., et al. 2006, A&A in preparation
[11] Saastamonien J. 1973, Bull. Géodésique 105, 279
[12] Chao C.C. 1974, in *The troposphere calibration model for Mariner Mars 1971*, *JPL/NASA Tech. Rep.*, 32-1587, 61
[13] Marcaide J.M., Elósegui P., Shapiro I.I. 1994, AJ 108, 368
[14] Blandford R.D., Königl A. 1979, ApJ 232, 34